sentation of the diatomic potential satisfying all of the available molecular data (*6, 8, 30*).
14. K. S. Jhung, I. H. Kim, K.-H. Oh, K. H. C. Jhung, *Phys. Rev. A* **44**, 4734 (1991).
15. K. P. Huber and G. Herzberg, *Molecular Spectra and Molecular Structure* (Van Nostrand Reinhold, New York, 1979), vol. 4; see also the references in (*8*) and reference 9 in (*14*).
16. In our analysis, we assume that the linear Hugoniot relation $U_s = C + Su_p$ holds, where U_s is the shock-wave velocity and u_p the particle velocity, and use the Mie-Gruneisen thermal correction, $\gamma/V = (\partial P/\partial E)_V$, where γ is the Grüneisen parameter [see (*20, 21*) for the data reduction and (*31, 32*) regarding γ].
17. A. Banerjea and J. R. Smith, *Phys. Rev. B* **37**, 6632 (1988).
18. F. Birch, *Phys. Rev.* **71**, 809 (1947); *J. Geophys. Res.* **83**, 1257 (1978).
19. P. Vinet, J. Ferrante, J. R. Smith, J. H. Rose, *J. Phys. C* **19**, L467 (1986).
20. R. Jeanloz, *J. Geophys. Res.* **94**, 5873 (1989). One can obtain cohesive energies from the equations of state by taking the limit $V \rightarrow \infty$ [the corresponding finite-strain parameter (*18*) $f \rightarrow -1/2$]; that is, we extrapolate the condensed-matter equations of state to infer the energy at infinite expansion. Note that the Universal equation of state yields more satisfactory values for the cohesive energy than does the Birch-Murnaghan equation of state (Fig. 4).
21. A. L. Ruoff, *J. Appl. Phys.* **38**, 4976 (1967).
22. The analysis involves reduction of the shock-wave data by the same approach described above (*10, 20*), along with the assumption that γ/V is constant [see (*33*) for data reduction]. The reason we calculated the energy change along the isentrope was that this minimizes the assumptions involved in the thermal correction from the Hugoniot state. Of course, if we had used zero-temperature values for the material variables, we would have obtained the conventional cohesive binding-energy relation as a function of distance. In our analysis, we also restricted the volume (or interparticle distance) to less than that at the ideal critical point, that is, the minimum point of the reduced isentrope, where the bulk sound speed goes to zero. At this point, the material no longer transmits sound waves, which implies that the ideal tensile strength has been exceeded (*34*).
23. Use Eq. 5 to cancel the second term on the right side of Eq. 4.
24. H. M. Hulburt and J. O. Hirschfelder, *J. Chem. Phys.* **9**, 61 (1941).
25. The pressure-volume (*P-V*) relation, expressed in reduced form, is

$$P_R = P/(E_0\,\partial z/\partial V) = -dF/dz = 2\exp(-z)$$
$$[\exp(-z)-1] + c\,(az-3)z^2\exp(-az)$$

with terms defined in Eq. 9. In analyzing the data, we made thermal corrections to Δ and β_1 through E_0, B_0, and B_0' (*35*): we considered both the lattice vibrational and electronic contributions to the thermal energy, the first being approximated by a Debye model (*36, 37*).
26. H. K. Mao, P. M. Bell, J. W. Shaner, D. J. Steinberg, *J. Appl. Phys.* **49**, 3276 (1978).
27. D. L. Heinz and R. Jeanloz, *ibid.* **55**, 885 (1984).
28. J. A. Morgan, *High Temp. High Pressures* **6**, 195 (1974).
29. M. S. Anderson and C. A. Swenson, *Phys. Rev. B* **28**, 5395 (1983); *ibid.* **31**, 668 (1985).
30. J. Ferrante, H. Schlosser, J. R. Smith, *Phys. Rev. A* **43**, 3487 (1991).
31. *Los Alamos Scientific Laboratory Report LA-4167-MS* (Los Alamos, NM, 1969).
32. S. N. Vaidya and G. C. Kennedy, *J. Phys. Chem. Solids* **32**, 951 (1971).
33. F. E. Prieto and C. Renero, *ibid.* **37**, 151 (1976); E. S. Lee, S. S. Lee, K. S. Jhung, I. H. Kim, *Korean J. Appl. Phys.* **2**, 121 (1989).
34. R. G. McQueen and S. P. Marsh, *J. Appl. Phys.* **33**, 654 (1962).
35. J. Berger and S. Joigneau, *C. R. Acad. Sci. Paris* **249**, 2506 (1959).
36. V. N. Zharkov and V. A. Kalinin, *Equations of State for Solids at High Pressures and Temperatures* (Consultants Bureau, New York, 1971).
37. L. V. Al'tshuler, S. B. Kormer, A. A. Bakanova, R. F. Trunin, *Sov. Phys. JETP* **11**, 573 (1960).
38. S. P. Marsh, Ed., *LASL Shock Hugoniot Data* (Univ. of California Press, Berkeley, 1980).
39. H. C. Rodean, *J. Chem. Phys.* **49**, 4117 (1968).
40. This work was supported by the National Aeronautics and Space Administration and the National Science Foundation.

3 September 1992; accepted 18 February 1993

Rates of Electron Emission from Negatively Charged, Impact-Heated Fullerenes

Chahan Yeretzian, Klavs Hansen, Robert L. Whetten

Thermal emission of electrons is ordinarily considered to be exclusively a property of macroscopic condensed matter. Slow electron emission occurs for certain small metal clusters as well as for silicon and carbon clusters, but the nature of this process has not been established. Electron emission rates have been obtained and analyzed from extensive real-time measurements on negatively charged fullerenes for several sizes and over a wide, continuous range of energies. These results confirm that delayed electron emission is a simple activated process that depends strongly on the internal energy and size of the cluster and that it has a common underlying mechanism, independent of size. However, the Arrhenius form deduced is inconsistent with the emission rate theory used for bulk surfaces. These results allow the question of the correct microscopic description of this newly observed electron emission process to be assessed.

Electron emission from an excited atom or molecule is considered a prompt process, occurring on an electronic time scale (10^{-16} s), except where particular autoionizing resonances are involved (*1*). On the other hand, condensed matter—for example, a tungsten filament—may exhibit thermal emission, characterized by activated rates that increase smoothly with excitation energy or temperature; the statistical rate theory of thermionic emission gives a successful microscopic description of this process (*2*). Several recent reports have documented observations of slow electron emission from strongly bound atomic clusters including tungsten (*3*), carbon (*4, 5*), and silicon (*6*); this discovery is considered promising in terms of attempts to develop a thermometry of clusters and is thought to reflect the emergence of bulk-like electronic structure. The recent examples of slow electron emission from large molecules and clusters are suggestive of a nonprompt emission mechanism, similar to emission from conducting surfaces. When strongly excited, by subthreshold radiation or by surface impact or atom bombardment, the neutral clusters of these elements cool through emission of an electron, either in competition with fragmentation or in its place. In an extreme case, irradiation of giant positively charged fullerenes, C_n^+ ($n > 200$), suspended in a magnetic trap, generates doubly charged molecules (C_n^{2+}), evidently by slow electron emission (*7*).

In the case of negatively charged clusters and negative molecular ions, it is less unusual that electrons are emitted preferentially to fragmentation, given that electron affinities often lie well below the fragmentation thresholds (*8*). Smalley and co-workers (*9*), in attempted photoelectron spectrum measurements, found that hot or multiphoton-excited C_{60}^- gives very broad time-of-flight (TOF) profiles limited only by the ion transit through the instrument. At the same time, it was reported that the electron emission peak arising from surface scattering of C_{60}^- (*10*), small carbon (C_n^-), or small silicon (Si_n^-) clusters (*6*) is strongly broadened at the threshold impact energy for electron ejection.

These reports raise unresolved questions regarding the nature of delayed emission in larger negatively charged atomic clusters, including whether a single rate can be defined and whether the process is thermally activated and describable by rate expressions already put forward. In particular, one would like to know how the rate depends on the cluster energy content and on the characteristics of the system, including electron affinity, size, and the spectrum of electronic excited states as well as the electron-ion coupling. Since the early days of activated rate theory, the precise measurement of the preexponential factor and the temperature dependence of the rate constant of specific unimolecular reactions have revealed the key information needed to deduce the underlying mechanism. The goal of our work has been to provide the necessary experimental information and to stimulate the development of appropriate physical models.

Department of Chemistry and Biochemistry, University of California, Los Angeles, CA 90024–1569.

In this report we describe a series of experiments in which negatively charged fullerenes are heated by impact with a solid surface and the charged scatterers are detected by TOF methods. This method of heating has advantages over laser or fast-atom excitation because the energy is coupled directly into vibrations rather than electronic excitations, the excitation energy is more narrowly defined, and the energy can be varied continuously over a large excitation range. The electrons generated as a consequence of low-speed impact (<14 km/s) are emitted from the intact, negatively charged cluster that has been scattered. The time-of-emission is long and can be observed in real time over a wide time window. The mean emission time, or rate, has been evaluated as a function of impact energy for several sizes and is shown to exhibit a sensitive dependence on both energy and size. These results allow the question of the correct statistical description of the electron emission process to be assessed.

The experimental arrangement is shown schematically in Fig. 1 (*11*). The beam is formed by laser desorption of fullerene films into a pulsed helium jet at 266 nm. Ions are extracted normal to the jet flow axis by a pulsed field and typically have an energy spread of ±6 eV for singly charged clusters. A mass-selected packet from the distribution is transmitted by a pulsed-mass gate, shown at the left-hand side of Fig. 1, and passes into the ultrahigh vacuum chamber before being decelerated to the desired impact energy at the surface, a Si(111) wafer. The surface is prepared by HF etching and is heated in vacuum to drive off molecular adsorbates; however, the scattering results reported here are from the silicon-oxide passivation layer. The reflected cluster beam, and other particles of the same charge, are accelerated toward the detector, which is mounted at a fixed angle of 10° with respect to the incident beam axis. The angle is rotated to compensate for the loss of parallel momentum in the collision so that efficient collection occurs at the 6-cm^2 area detector. The results presented below are recorded under conditions where the normal component of the impact energy is 50 eV or greater; with the beam energy set to 1.8 keV, the parallel component is typically near 40 eV. The angle of impact is always less than 45° from the surface normal and moves rapidly toward normal with increasing impact energy. We follow convention below in referring to the normal component alone as the impact energy.

Our results are illustrated by Fig. 2, where typical TOF profiles are shown for the scattering of mass-selected C_{70}^- from a silicon surface. We identify three main features from the apparatus calibration. First, the C_{70}^- peak is at far right and corresponds to the intact scattering channel arriving at the detector some 10 μs after collision, with only a small time shift associated with the recoil velocity (*10*). Second, there is a small peak of constant intensity and location at far left, corresponding to electrons emitted—and instantaneously detected (<10^{-7} s)—by high-energy impact of a small fraction of the incoming beam with the entrance grid of the deceleration field. Third, there is a signal that has an onset coinciding precisely with the time-of-impact and whose profile changes strongly with impact energy. This signal corresponds to electrons emitted as a result of the collision, rather than photons, as it is sensitive to electric fields near the detector. The profile is abruptly truncated at 1.4 μs after the impact, as measured from the midpoint of the rise to the end of the profile. This value is slightly less than the calculated time-of-travel of C_{70}^- through the field region at that acceleration potential, neglecting recoil velocity. Similar results have been obtained for a number of different fullerenes (n = 58, 60, 70, 80, and 96).

A series for the cluster sizes n = 60, 70 (Fig. 2), and 96 have been measured in detail. The most important feature of these electron emission TOF profiles is their sensitive dependence on the impact energy. The profile width is given in all cases by the ion residence time in the accelerating field, from which it follows that electrons are emitted from the scattered ions all throughout their flight through this spatial region. If the scattered C_n^- ions survive their flight through this region without emitting an electron, then the free-flight velocity is determined, so that the ions and subsequently emitted electrons are detected at the total flight time of the ion. If, on the other hand, an electron is emitted from a scattered C_n^- at some location in the accelerating region, then the electron provides an essentially instantaneous report of the emission event. This difference results from the electron mass being ~10^6 times less than the mass of C_{60}, so that a typical 10^{-5} s TOF for a fullerene translates to a 10^{-8} s electron TOF—instantaneous in our apparatus. Consequently, the observed electron intensity profile, $p(t)$, reflects directly the electron emission probability from impact-heated fullerenes as a function of time and is expressed by

$$p(t) = -\frac{d[I_n(t)]}{dt} \qquad 0 < t < \tau_0$$

$$= 0 \; t < 0, \; t > \tau_0 \qquad (1)$$

where $I_n(t)$ is the C_n^- intensity at a delay time t after impact and τ_0 is the ion flight time in the accelerating region.

The emission profiles presented in Fig. 2 show that delayed emission occurs from the negatively charged fullerene C_n^- after it scatters from the surface, at impact energies up to ~4 eV/atom. The processes observed can thus be represented by the sequence

$$C_n^- \xrightarrow{\text{Impact}} C_n^{-*} \xrightarrow{t} e^- + C_n^{(0)} \qquad (2)$$

where t is the delay time. This process occurs in competition with dark processes, such as sticking or electron transfer, involving loss of charge to the surface

$$C_n^- \xrightarrow{\text{Impact}} e^-_{(\text{surface})} + C_n^{(0)}{}_{(\text{surface or vacuum})} \qquad (3)$$

which is dominant >300 eV in the case of fullerene collisions with silicon surfaces, and is not analyzed further here.

The analysis of the emission rates is

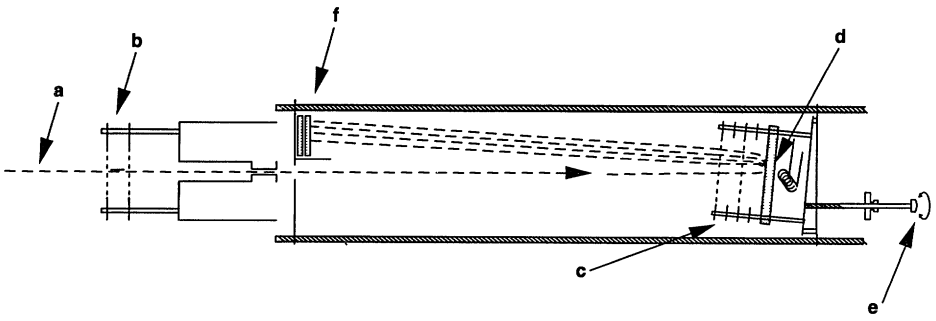

Fig. 1. Diagram of the apparatus, with detail of the impact region. The ionized fullerene beam (**a**) is generated by laser desorption (fourth harmonics of a Q-switched Nd:YAG laser; 266 nm) and swept along in a pulsed helium flow through the skimmer and into the pulsed extraction region of a pulsed reflectron TOF mass spectrometer. The negative ions are extracted perpendicular to the gas flow, focus by a Einzel-lens, and mass-selected in a temporal mass-gate (**b**). After 20 cm of free flight, the monodisperse ion beam enters a 1.4-cm retarding field (**c**), where it is slowed down to the desired momentum of impact before colliding with the surface (**d**). The scattered, charged particles are accelerated in the same field toward the detector (**f**). The angle between incoming ion-beam and acceleration is fixed at 10°, whereas the impact angle can be optimized by a mechanical drive (**e**) for optimal collection efficiency of either the reflected or the scattered beam.

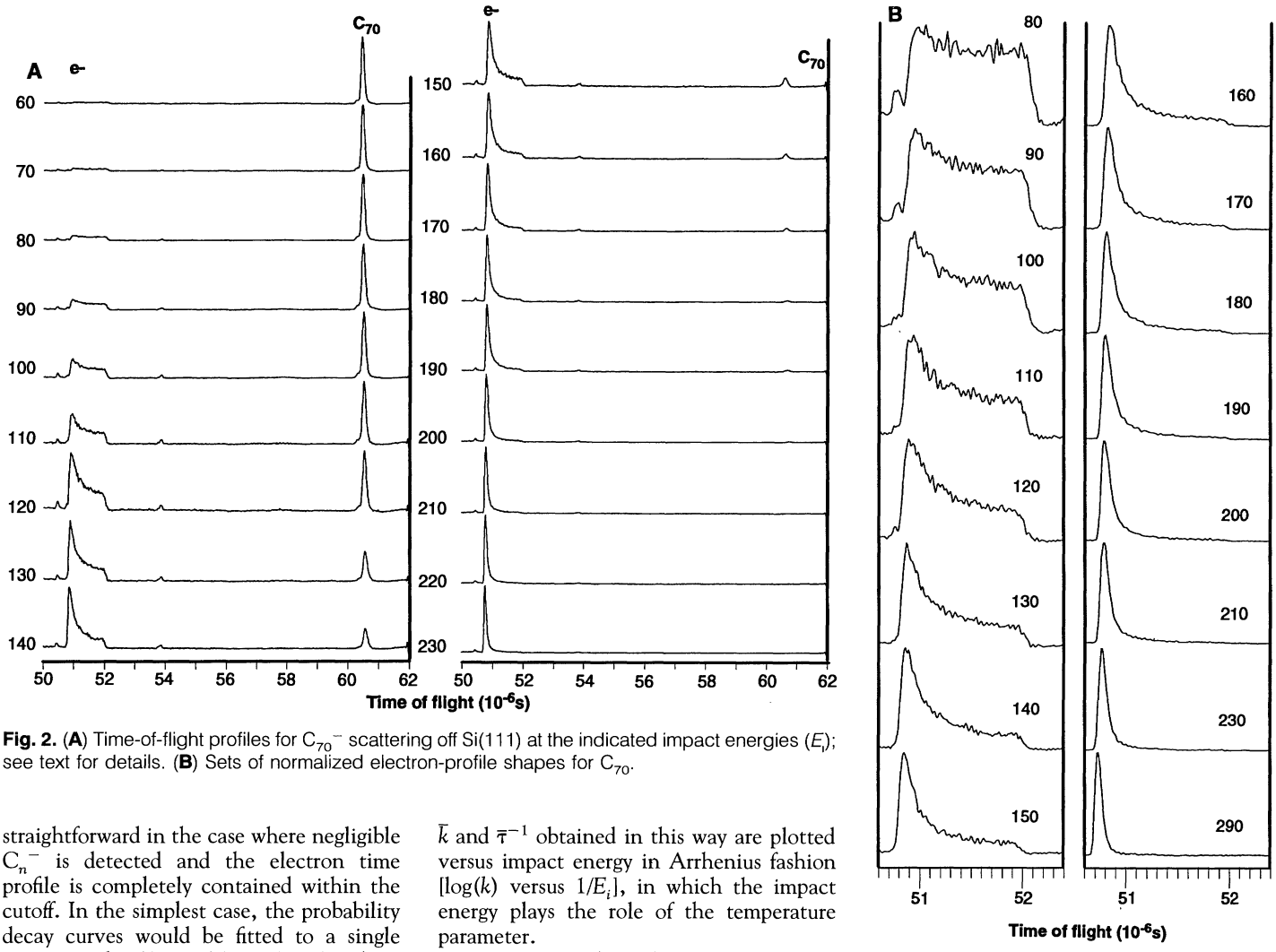

Fig. 2. (**A**) Time-of-flight profiles for C_{70}^- scattering off Si(111) at the indicated impact energies (E_i); see text for details. (**B**) Sets of normalized electron-profile shapes for C_{70}.

straightforward in the case where negligible C_n^- is detected and the electron time profile is completely contained within the cutoff. In the simplest case, the probability decay curves would be fitted to a single exponential, $p(t) = p(0)\exp(-t/\tau)$, where τ is the emission lifetime. However, we find that the profiles cannot be adequately represented by single exponentials, and so have adopted two more general measures to obtain mean survival times, $\bar{\tau}$, and mean decay rates, $\bar{k}$. It can be shown that, given an arbitrary (normalized) distribution of single exponential decay rates, $\rho(k)$, then the mean rate, defined by $\bar{k} = \int dk \cdot k \cdot \rho(k)$, is given by

$$\bar{k} = \frac{p(0)}{\int dt \cdot p(t)} \quad (4)$$

When the decay is not too fast, we find that this simple formula gives a robust value for $\bar{k}$. For very fast decays, an expression for the mean time-of-decay may be more appropriate

$$\bar{\tau} = \frac{\int dt \cdot t \cdot p(t)}{\int dt \cdot p(t)} \quad (5)$$

where the time-zero can be set at the peak maximum so as to remove the effect of the (symmetrical) instrumental peakwidth. In Fig. 3 some values for n = 60, 70, and 96 of $\bar{k}$ and $\bar{\tau}^{-1}$ obtained in this way are plotted versus impact energy in Arrhenius fashion [$\log(k)$ versus $1/E_i$], in which the impact energy plays the role of the temperature parameter.

A more complicated case arises when a significant fraction of the signal is outside the window, that is, when there is a significant C_n^- peak remaining. Equation 4 could still be used, with the denominator representing the total scattered C_n^- as well, but the detector sensitivity for electrons versus fullerene negative ions is not known a priori. We have obtained an empirical estimate of the ratio of detector sensitivities by assuming that the total yield of scattered negative fullerenes should be a smoothly and slowly varying function of impact energy over the range of interest here, that is, that the fraction of losses through process 3 does not vary strongly over that range. In this case, the strong decrease in integrated C_n^- signal is correlated with the strong increase in integrated e^- signal, and it is found that the collection-detection efficiency is ~4 times higher for electrons as for fullerenes. [Support for a slow variation comes from analogous experiments on positively charged fullerenes, C_n^+, which show only a very gradual decrease in integrated intensity across the impact energy range from 80 to 180 eV (*4*).] We have used this factor, β = 4, in the expression

$$\bar{k} = \frac{p(0)}{\int dt \cdot p(t) + \beta \cdot I_n(t = \tau_0)} \quad (6)$$

to obtain the values for the mean rate versus E_i plotted as solid points in Fig. 3.

The results presented in Fig. 3 give a quantitative picture of the delayed emission of electrons from molecule-sized systems and allow a number of assertions to be tested. In considering these, we take the view that the delayed emission curves represent rates of emission from impact-heated fullerenes, at times long after the time-of-contact with the surface, and hence reflect intrinsic molecular rates, $k(U)$, depending only on the cluster internal energy U. The nonexponential character of the curves reflects a distribution of rates, $\rho(k)$, derived from some spread of energies, $U \pm \delta U$, imparted by impact. The following conclusions can be made.

First, the rate of emission is a strong function of the impact energy, with the rates varying by nearly three orders of magnitude when the energy is tripled. In Fig. 3,

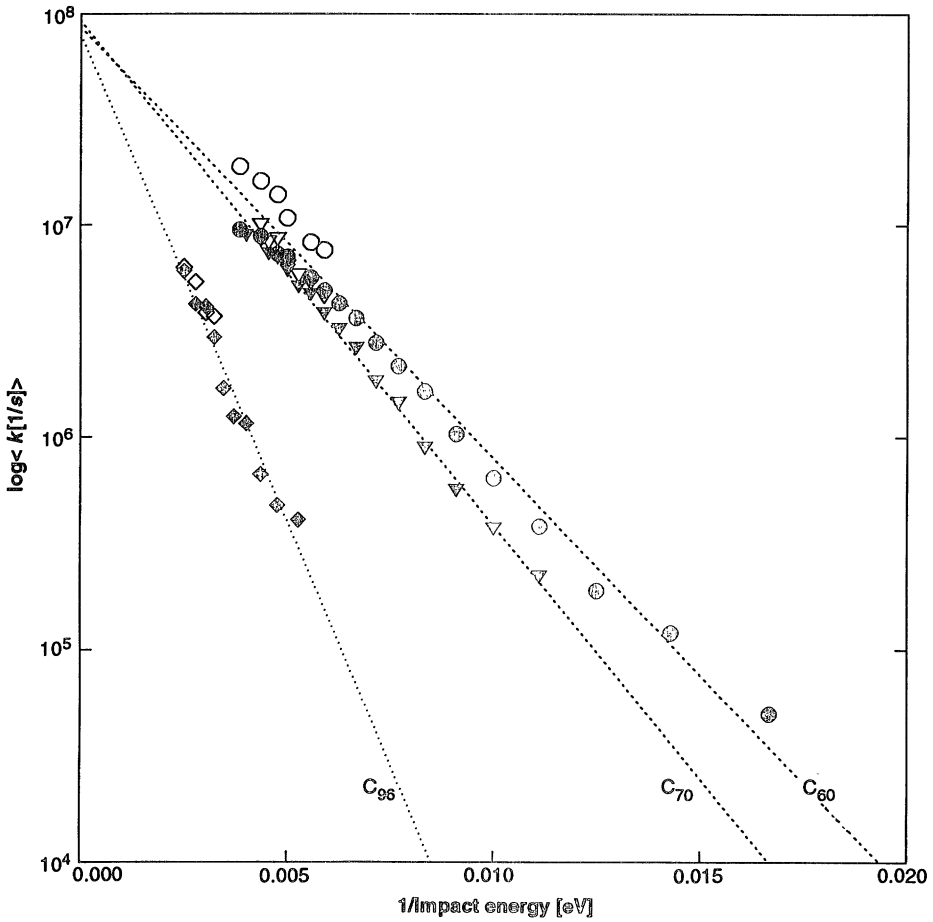

Fig. 3. The mean rate-constants of electron emission from impact-heated fullerenes are plotted as $\log(\overline{k})$ versus impact energy in Arrhenius fashion. The data points are C_{60} (circles), C_{70} (triangles), and C_{96} (diamonds), as determined by methods described in the text by using Eq. 6 (filled symbols) or Eq. 5 (hollow symbols).

the rates are plotted versus impact energy in Arrhenius fashion, $\log(k)$ versus $1/E_i$, implicitly testing the ansatz

$$k(E_i) = A \cdot \exp\left(\frac{-E_a}{\lambda E_i}\right) \qquad (7a)$$

in which the impact energy plays the role of the temperature parameter and the prefactor A and activation energy E_a have the usual meaning. The linear behavior of the Arrhenius plot confirms that the process is indeed activated and that the impact energy determines the cluster temperature. For electron emission, the activation energy is evidently the electron affinity of C_{60} or C_{70}, 2.65 eV (9). The dimensionless parameter λ converts the impact energy into the effective temperature (k_BT) of the molecule, $\lambda = s/\alpha$, where $\alpha = U/E_i$ is the fraction of the impact energy imparted to the cluster's internal energy, and $s = 3n - 6$ is the number of vibrational modes in the n-atom molecule

$$k(E_i) = A \cdot \exp\left(\frac{-sE_a}{\alpha E_i}\right) \qquad (7b)$$

For example, for C_{70} one derives a slope near 300 eV^{-1} and an intercept $A \approx 10^8$ s^{-1} or 10^9 s^{-1} (depending on whether the normal component or the total beam energy is taken for E_i). From the observed slope and the known electron affinities, one obtains $\alpha \approx 0.5$ (*12*). The mechanism of molecular excitation from hyperthermal surface impact is well understood empirically and by simulations. The impact energy, E_i, is partitioned into a small recoil kinetic energy (*13*), surface-heating, and cluster-heating U, where we neglect the prior energy content of the cluster. A fairly well-defined (and nearly constant) fraction, α, is converted into heating the scattered molecule or cluster, that is, $\alpha = U/E_i$. For medium-sized molecules, α is in the 0.10 to 0.15 range, but for compact projectiles with many more atoms the values are larger, α is in the 0.15 to 0.3 range. The limiting value is 0.5 for large-cluster impacts. Simulations of C_{60} impact against hydrogen-terminated diamond (111) in the 150 to 250 eV range give $\alpha = 0.24$ to 0.27, with little dependence on E_i (*14*). [A statistical spread in the internal energy U, deduced from the number of degrees of freedom in the scattered cluster, $\delta U/U \approx s^{-1/2}$, would account for the nonexponential decay curves found (*15*).]

Second, at a given impact energy, the rate decreases strongly with size. This is also explained by the Arrhenius formulation (Eq. 7b). When plotted against s/E_i, the rate plots for C_{60} and C_{70} (with identical electron affinities) now overlap with identical slopes, within the scatter of the data. This result further establishes that the temperature of the molecule (energy per atom) is the controlling parameter. The plot for C_{96} has a 40% greater slope, suggesting that the electron affinity is higher, near 3.7 eV.

Third, the high-temperature intercept of these plots are all near 10^8 s^{-1}, suggesting a common underlying mechanism. However, this value is *not* consistent with the predictions of the statistical rate theory of thermionic emission from uniform surfaces of metals, which assumes a thermal equilibrium population over a continuum (Fermi-Diract distribution) of energy levels. The Richardson equation expresses the electron emission current per unit surface area, j, as a function of temperature T, in terms of the work function ϕ and a reflection coefficient, r (*2*)

$$j = A(1 - r)T^2\exp\left(\frac{-\phi}{k_BT}\right) \qquad (8a)$$

where A is a constant that has the theoretical value 120 A cm^{-2} K^{-2}. A modification (*16*) of this equation for finite-sized systems expresses the rate constant as

$$k(T) = \frac{2k_BT}{h}$$
$$\{2b/a_0 + Q_s + (\pi Q_s)^{1/2}\}\exp\left(\frac{-\phi}{k_BT}\right) \qquad (8b)$$

where b is the geometrical radius of the cluster and the dimensionless quantity $Q_s = 2m_eb^2k_BT/h^2$. Where m_e is the electron mass and h is Planck's constant. With the C_{60} collision radius $b/a_0 = 10$ and $T = 3000$ K, this gives $Q_s = 2$, so that the first term in the bracket is dominant. This approach yields only a slight modification to the results from Eq. 8a; the prefactor is near 10^{15} s^{-1}, in gross disagreement with the intercept found in Fig. 3. [A second formula, explicitly written for emission from negative ions (*16*), gives a series that fails to converge, with the parameters for C_{60}.]

These considerations indicate that the statistical rate theory of electron emission, as commonly formulated and universally invoked, is inappropriate for negatively charged fullerenes. It is therefore necessary to examine alternative formulations that better incorporate the electronic excitations of negatively charged clusters. In the case of C_{60}^-, at least, there is a good deal of

information about the sparse spectrum of excited states below the emission threshold at 2.7 eV. It may be that after impact imparts energy into the vibrational degrees of freedom, leaving the electrons initially in the ground state, the rate-limiting step is the vibration-to-electronic excitation process. In this case, the appropriate prefactor is an electron-vibrational coupling constant, determined here to be near or somewhat larger than 10^8 s^{-1}. Other hypotheses have been proposed in order to account for low ionization efficiencies of large molecules (*17*).

To establish the nature of a rate process, and thereby to obtain a correct microscopic theory, it is necessary to measure the rate as a function of energy or temperature. In this report we have presented this crucial information for delayed emission of electrons from large molecules. The generality of these conclusions, derived from experiments on negatively charged fullerenes, should be examined for other cluster and molecular systems that show thermionic emission. One very interesting question is the evolution with size toward the bulk limit (Richardson equation), which in the case of fullerenes should tend toward the properties of graphite (a semimetal), and in clusters of elements like tantalum or tungsten should tend toward the properties of the bulk metal.

REFERENCES AND NOTES

1. C. Y. Ng, *Adv. Chem. Phys.* **52**, 263 (1983).
2. C. Herring and M. H. Nichols, *Rev. Mod. Phys.* **21**, 185 (1949).
3. T. Leisner *et al.*, *Z. Phys.* **D20**, 127 (1991); A. Amrein, R. Simpson, P. A. Hackett, *J. Chem. Phys.* **95**, 1781 (1991); *ibid.* **94**, 4663 (1991).
4. C. Yeretzian and R. L. Whetten, *Z. Phys.* **D24**, 199 (1992).
5. E. E. B. Campbell, G. Ulmer, I. V. Hertel, *Phys. Rev. Lett.* **67**, 1986 (1991).
6. P. M. St. John and R. L. Whetten, *Chem. Phys. Lett.* **196**, 330 (1992); P. M. St. John, C. Yeretzian, R. L. Whetten, *J. Phys. Chem.* **96**, 9100 (1992).
7. S. Maruyama, M. Y. Lee, R. E. Haufler, Y. Chai, R. E. Smalley, *Z. Phys.* **D19**, 409 (1991).
8. R. F. Foster, W. Tumas, J. I. Brauman, *J. Chem. Phys.* **79**, 4644 (1983).
9. L.-S. Wang, J. Conceicao, C. Jin, R. E. Smalley, *Chem. Phys. Lett.* **182**, 5 (1991).
10. R. D. Beck, P. M. St. John, F. Diederich, R. L. Whetten, *J. Phys. Chem.* **95**, 8402 (1991).
11. R. D. Beck, P. M. St. John, M. L. Homer, R. L. Whetten, *Science* **253**, 879 (1991).
12. This value for α has to be seen as an upper bound and will be reduced somewhat when considering the parallel momentum loss and also the thermal energy content in the incident beam. Furthermore, the limit $\alpha \leq 0.5$ should only hold for the case of surface and ion composed of similar materials.
13. Only at low energies ($E_i < 50$ eV) is the collision significantly elastic, with recoil kinetic energy accounting for >10% of the impact energy: C. Yeretzian, K. Hansen, R. D. Beck, R. L. Whetten, *J. Chem. Phys.*, in press, H.-G. Busmann, Th. Lill, I. V. Hertel, *Chem. Phys. Lett.* **187**, 459 (1991).
14. R. C. Mowrey, D. W. Brenner, B. I. Dunlap, J. W. Mintmire, C. T. White, *J. Phys. Chem.* **95**, 7138 (1991).
15. On the basis of such nonexponential decays, it has even been questioned whether the assumption of an activated rate is warranted: G. Walder and O. Echt, in *Clusters and Fullerenes*, V. Kumar and E. Tosatti, Eds. (World Scientific, Singapore, in press).
16. C. E. Klots, *Chem. Phys. Lett.* **186**, 73 (1991).
17. E. W. Schlag and R. D. Levine, *J. Phys. Chem.* **96**, 10608 (1992).

18. This research was supported by the U.S. Office of Naval Research. R.L.W. and C.Y. acknowledge grants from the Packard Foundation and the Swiss National Science Foundation, respectively.

12 January 1993; accepted 9 March 1993

Van der Waals Epitaxial Growth of α-Alumina Nanocrystals on Mica

S. Steinberg, W. Ducker, G. Vigil, C. Hyukjin, C. Frank, M. Z. Tseng, D. R. Clarke, J. N. Israelachvili*

Lattice mismatch stresses, which severely restrict heteroepitaxial growth, are greatly minimized when thin alumina films are grown by means of van der Waals forces on inert mica substrates. A 10-nanometer-thick epitaxial film exhibits crystallographic sixfold symmetry, a lattice constant close to that of the basal plane [0001] of α-alumina (sapphire), and an aluminum:oxygen atomic ratio of 1:1.51 ± 0.02 (measured by x-ray photoelectron spectroscopy), again the same as for bulk sapphire. The film is free of steps and grain boundaries over large areas and appears to be an ideal model system for studying adhesion, tribology, and other surface phenomena at atomic scales.

The potential for new materials with tailored bulk, surface, and interface properties has stimulated extraordinary interest during the past 20 years, particularly in the field of ceramic materials. Ceramics have been designed with specialized physical properties for use in electronic, optical, nuclear, and structural applications (*1*). As a typical structural ceramic, sapphire (the single-crystal form of α-alumina, Al_2O_3) shows a combination of interesting properties such as great hardness, high wear resistance, chemical inertness, and high electrical resistivity. Because of its outstanding biocompatibility and high compressive strength, high-purity alumina also serves as an excellent implant material in human prosthetic devices (*2*).

These demands and other potential applications have motivated recent investigations into the correlations between composition and the electronic and surface structure of Al_2O_3 in its various phases (*3–5*). However, less progress has been made toward developing pure sapphire crystals of homogeneous (crystalline) microstructure, free of defects and with an extremely smooth surface—that is, with a mean surface roughness in the subnanometer range. In an attempt to address these issues and in consideration of the need for using oxide materials as thin films for microdevices, we investigated the possibility of epitaxially growing thin sapphire films on mica. "Breaking the mica barrier" by seeking other crystalline surfaces that can be easily prepared as thin, semitransparent layers suitable for use in the surface forces apparatus (*5–8*) could increase our understanding of adhesion, friction, and colloidal interactions.

We used the van der Waals epitaxy (VDWE) method recently developed by Koma *et al.* (*9*) for growing two-dimensional layered materials on a variety of substrate surfaces that need not be epitaxially well matched to the layers being grown. In this method, film growth is initiated by the relatively weak and nonspecific van der Waals forces between the film and saturated substrate molecules (that is, substrate surfaces having no dangling bonds), which produces unstrained films that can be grown to thicknesses of 5 to 20 nm while their intrinsic crystalline structure is preserved. Koma *et al.* (*9*) showed that the VDWE method is very effective for growing heterostructures even when the lattice mismatch between the film and substrate lattices is as high as 10%, with one reported case—$MoSe_2$ on mica—where the lattice mismatch was 58% (*10*). If extended to other metal oxide, mineral, and ceramic surfaces, the possibility of obtaining relatively thick, defect-free films with crystalline structures that are the same as in the bulk material would represent a significant improvement over conventional molecular beam epitaxy and chemical vapor–deposited coatings, which cannot produce such layers unless the film–substrate lattice mismatch is less than ~1% (*11–15*). Other growing meth-

S. Steinberg, W. Ducker, G. Vigil, J. N. Israelachvili, Department of Chemical and Nuclear Engineering, University of California, Santa Barbara, CA 93106.
C. Hyukjin and C. Frank, Department of Chemical Engineering, Stanford University, Stanford, CA 94305.
M. Z. Tseng, Department of Electrical and Computer Engineering, University of California, Santa Barbara, CA 93106.
D. R. Clarke, Materials Department, University of California, Santa Barbara, CA 93106.

*To whom correspondence should be addressed.